Chapter 2
Physics of the Tunable Ferroelectric Devices

Abstract This chapter gives an introduction to those aspects of the theory of ferroelectricity that a microwave engineer needs for understanding the physics behind tunable microwave devices. In spite of the simplicity the provided theory is quite useful for designing microwave devices and the interpretation of the experimental results. The crystalline structure of the displacive perovskite ferroelectrics, the DC field dependent dielectric permittivity and loss tangent are in the focus. The dynamic nonlinearity and acoustic properties are also considered.

2.1 Introduction

Crystalline, dielectric and electroacoustic properties of ferroelectrics are briefly reviewed in this chapter. The main focus is on crystalline/polycrystalline ferroelectrics with perovskite structure. Perovskite ferroelectrics are extensively studied in the past. They are rather well understood and commonly used in tunable microwave devices. Ferroelectrics used in tunable microwave devices may have one of the following forms:

- Single crystal ($SrTiO_3$, $KTaO_3$ etc.):
  - Bulk
  - Thin film
- Single phase (i.e. $Ba_xSr_{1-x}TiO_3$) and composite (i.e. $MgO+SrTiO_3$) ceramics:
  - Bulk-granular
  - Thick film (HTCC, LTCC)-granular
  - Thin film-granular, columnar

i.e. they have either single crystal, granular or columnar structure. The amorphous ferroelectrics, typically thin films deposited at low/room temperatures, are used in passive none tunable MIM capacitors. They are not considered in this chapter. The

same ferroelectric composition (i.e. $SrTiO_3$) may have different dielectric properties depending not only on the structure (single crystal, granular or columnar), but also on the mechanical strains. In the past relatively simple dielectric models based on thermodynamic and microscopic theories for the uniform single crystal (bulk, epitaxial film) ferroelectrics have been developed (Barrett 1952), (Ruprecht et al. 1961, Vendik and Zubko 1997). These models have been extended and applied to ceramics (granular, columnar, composite) ferroelectrics (Tagantsev et al. 2005). Quite recently the models based on the density function theory (DFT) are considered extensively. The DFT seems to be especially useful when it comes to nanostructured ferroelectric films and devices. The interested reader is refereed to adequate publications in this field (Chosez and Junquera 2006).

2.2 Crystal Structure, Non-Polar (Paraelectric) and Polar (Ferroelectric) Phases

The complex metal oxide ferroelectrics, i.e. perovskites such as Titanates ($CaTiO_3$, $BaTiO_3$ etc.), Tantalites ($KTaO_3$ etc.), Niobates ($KNbO_3$ etc.) etc. are characterized by a common chemical formulae, ABO_3, and have the same crystal structure (Fig. 2.2.1). Above polar-to-non-polar phase transition temperature their crystal lattice has cubic structure (Fig. 2.2.1 (a)). In this phase the crystal has no spontaneous polarization. Its permittivity is rather high, DC field, temperature and strain dependent. Below the phase transition temperature the crystal lattice becomes non cubic, non center-symmetric, the centers of the positive and negative charges per unit cell shift as shown Fig. 2.2.1 (b) and the crystal is characterized by spontaneous polarization. One for the surfaces of a macroscopic crystal is charged positively, while the opposite surface is charged negatively.

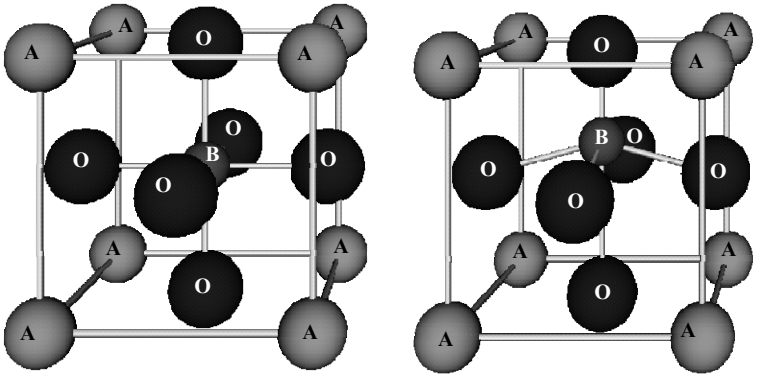

Fig. 2.2.1 3D unit cell of ABO_3 (e.g. $BaTiO_3$) perovskites in paraelectric (a) and polar-ferroelectric (b) phases

Figure 2.2.2 illustrates the 1D model of a perovskite crystal in paraelectric and ferroelectric phases. It is customary to represent the electrostatic interaction faces by mechanical springs. In these simplified models, in paraelectric-center-symmetric phase (Fig. 2.2.2 (a) and Fig. 2.2.2 (b)) the central ion oscillates about the equilibrium (x=0) and its free energy is characterized by a parabolic dependence (=kx^2, where k is the spring constant) as shown in Fig. 2.2.2 (a). An applied external electric field (along x axis) shifts the central ion from its equilibrium position inducing an electrical dipole. The ion continuous its oscillations about this new position with somehow less intensity (reduced permittivity). The ion comes back to its equilibrium position (x=0) as soon as the external field is switched off. This is the basic electric field tuning mechanism of the permittivity used, for example, in tunable microwave devices.

In polar, i.e. ferroelectric phase the positive ion is slightly shifted from the lattice center to the left (Fig. 2.2.2 (d)), or to the right (Fig. 2.2.2 (e)). In these two new positions the free energy of the crystal is minimum (Fig. 2.2.2 (c)). The ion remains in one of these two off-center poisons as far as no external forces (electrical, mechanical, temperature) are applied. It is characterized by an internal dipole, i.e. spontaneous polarization. Under external DC field the center ion may be switched from its left to its right position-changing the direction of the polarization vector (direction). Changing the direction of the external field brings the ion back to its left position-restoring the direction of the previous polarization. This is the main polarization switching/reversing mechanism used, for example, in memory cells.

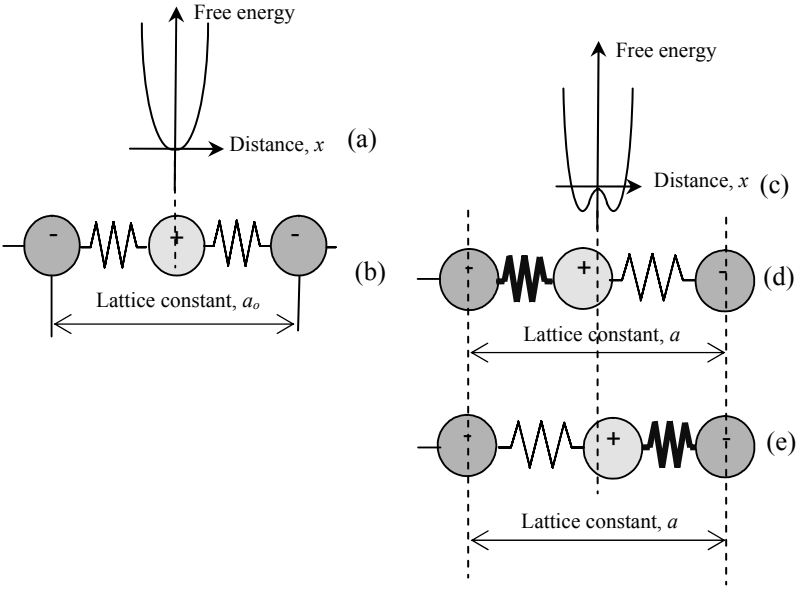

Fig. 2.2.2 Free energy destitution in 1D unit cells of ABO_3 (e.g. $BaTiO_3$) perovskites in paraelectric (a, b) and polar-ferroelectric (c, d, e) phases

2.3 Dielectric Models of the Ferroelectric and Paraelectric Phases

2.3.1 Phenomenological (Thermodynamic) Theory

This theory is based on the expansion of the free energy of a ferroelectric crystal as a function of polarization P (Tagantsev et al. 2005):

$$F(P,T) = \frac{1}{2}\alpha P^2 + \frac{1}{4}\beta P^4 \ldots \tag{2.3.1}$$

At this instance the higher order terms in this expansion are ignored. It contains only even terms to reflect the fact the free energy of the crystal dose not depended on the polarization reversal. The physical meanings of the dielectric permittivity and nonlinearity coefficients α and β are disclosed below. Notice that this relationship holds true both for paraelectric and ferroelectric (polar) phases. The first derivative of this function is:

$$\frac{\partial F(P,T)}{\partial P} = E = \alpha P + \beta P^3 \ldots \tag{2.3.2}$$

From the simple relationship between the electric field and polarization it becomes clear that the coefficient α should have a meaning of the inverse permittivity: $\alpha=1/(\varepsilon\varepsilon_o)$, where ε is the relative dielectric permittivity and ε_o is the dielectric constant of vacuum. Furthermore, taking into account the experimentally observed temperature dependence of the permittivity, i.e. the Curie-Weiss low, $\varepsilon=C/(T-T_{ph})$, the coefficient α takes the form:

$$\alpha = \frac{T - T_{ph}}{\varepsilon_o C} \tag{2.3.3}$$

C is the Curie constant and the temperature T_{ph} is equal or lower than the Curie temperature T_c. Its meaning will be clear a couple of lines below.

In polar (ferroelectric) phase the spontaneous polarization, P_s, is found when the externally applied electric field E=0, i.e. from (2.3.2) $\alpha P_s+\beta P_s^3 = P_s(\alpha+\beta P_s^2)=0$. The last equation has two solutions: P_s=0 and $(\alpha+\beta P_s^2)$=0. From the second solution, taking into account (2.3.3), one arrives at:

$$P_s = \sqrt{(T_{ph} - T)/(\beta\varepsilon_o C)} \tag{2.3.4}$$

which is valid below temperature $T=T_{ph}$. At $T=T_{ph}$ the spontaneous polarization P_s=0, i.e. T_{ph} is the phase transition temperature. Below this temperature the ferro-

electric is in polar (ferroelectric) phase with $P=P_s$. Above the ferroelectric is in paraelectric phase with $P_s=0$. In this case the paraelectric-to-ferroelectric phase transition is of the second order and the phase transition temperature is identical with the Curie-Weis temperature $T_c=T_{ph}$. For the first order phase transition (Vendik and Zubko 2000) the phase transition temperature is less than the Curie-Weiss temperature, $T_{ph}<T_c$.

The dielectric permittivity is given as:

$$\varepsilon = \frac{1}{\varepsilon_o}\frac{\partial E}{\partial P} = \frac{1}{\varepsilon_o(\alpha + 3\beta P^2)} \tag{2.3.5}$$

In paraelectric ($T>T_C=T_{ph}$) phase, and without external electric field, i.e. $P=0$, from (2.3.5) and (2.3.3) one gets Curie-Weiss low:

$$\varepsilon = \frac{C}{T - T_c} \tag{2.3.6}$$

For ferroelectric, polar phase ($T<T_C=T_{ph}$) the permittivity is found from (2.3.3)–(2.3.5):

$$\varepsilon = \frac{C}{2(T_c - T)} \tag{2.3.7}$$

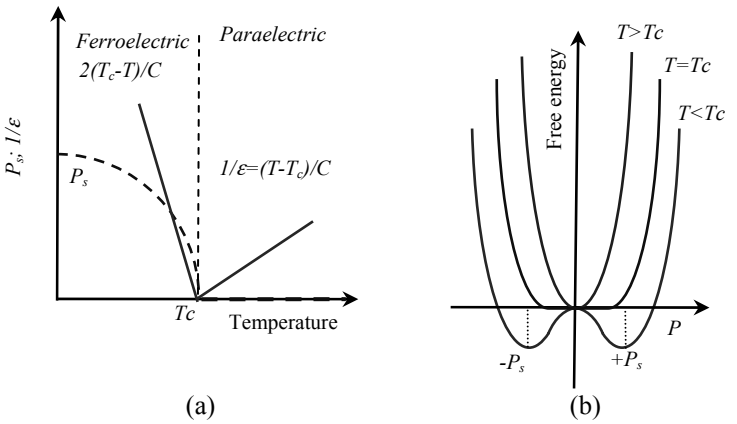

Fig. 2.3.1 2nd order paraelectric to ferroelectric phase transition. Temperature dependences of the polarization and inverse permittivity (a), and polarization dependent free energy (b)

The temperature dependences of the spontaneous polarization and inverse permittivity for a ferroelectric crystal with 2nd order phase transition, defined by (2.3.4), (2.3.6) and (2.3.7) are depicted in Fig. 2.3.1 (a). Figure 2.3.1 (b) depicts the dependences of the free energy on the polarization (2.3.1) for ferroelectric

($T<T_c$) paraelectric ($T>T_c$) and phase transition ($T=T_c$) temperatures. The two minima in ferroelectric phase correspond to two equilibrium states of the spontaneous polarization, shown previously in Fig. 2.2.2 (c), while the dependence with a single minimum (T>Tc) corresponds to the case shown in Fig. 2.2.2 (a).

The hysteresis (Fig. 2.3.2 (a)) with the two equilibrium polarization states is used to utilize nonvolatile memory cells. The corresponding permittivity-field dependence (computed using the derivative in (2.3.5)) is shown in Fig. 2.3.2 (b), where the maximums in permittivity appear at coercive field $\pm E_c$. In principle, this type of "butterfly" permittivity-field dependence may be used in analog tunable microwave varactors provided that the associated losses are small and the required tuning speeds are not high. In this case the bias field has to be increased from zero or decreased from E_{max} in order to establish the required permittivity on the given branch of the $\varepsilon(E)$ dependence. The polar phase with $\varepsilon(E)$ hysteresis may be used also as a microwave switch if the ratio $\varepsilon_m/\varepsilon_n$ of the permittivity at the points *m* and *n* (Fig. 2.3.2 (b)) is sufficient for the targeted application. Additionally, in polar phase all ferroelectrics also are piezoelectric and, as such, some of them are used in acoustoelectronic devices.

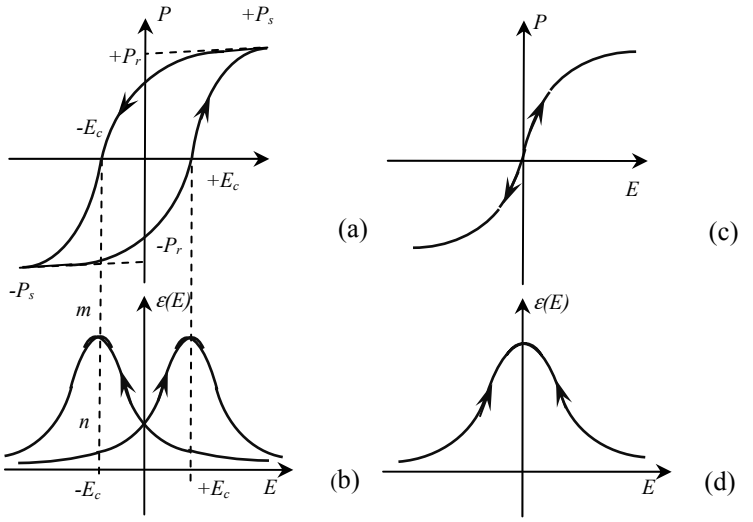

Fig. 2.3.2 Polarization (a and c) and permittivity (c and d) dependences on the applied electric field for ferroelectric (a and c) and paraelectric (b and d) phases

In paraelectric, $T>Tc$, phase the spontaneous polarization is zero and the inverse permittivity is a nonlinear function of the applied electric field (Fig. 2.3.1 (a)). At small bias fields the free energy is a parabolic function of the polarization (Fig. 2.3.1 (b)) as it appears in (2.3.5). The $P(E)$ dependence in this phase is again nonlinear but without hysteresis loop (Fig. 2.3.2 (c)). The $\varepsilon(E)$ performance is also essentially nonlinear (Fig. 2.3.2 (d)) and for small bias fields is characterized with a parabolic dependence, as shown below. In this phase, using

the relationship between polarization and applied field, $P=\varepsilon_o\varepsilon(0)E$, one gets from (2.3.5): $\varepsilon(0)=1/(\alpha\varepsilon_o)$. By using this results in (2.3.5) one arrives at

$$\varepsilon(E,T)=\frac{\varepsilon(0,T)}{1+3\beta\varepsilon_o^3\varepsilon^3(0,T)E^2} \tag{2.3.8}$$

where the temperature dependence of the permittivity at zero bias field, $\varepsilon(0,T)$, is given by (2.3.6).

2.3.2 Microscopic Theory

In general, the thermodynamic theory considered in the previous section does not care about the microscopic, ionic structure and chemical composition of the ferroelectric crystal. The change in crystal symmetry at phase transition is the only concept which the thermodynamic theory considers. The microscopic theories consider the chemical/ionic structure of a ferroelectric crystal and thermal oscillations (vibrations) of the ions about their equilibrium positions, and their interactions. The microscopic, dynamic theory of ferroelectrics is based on the vibrations of the ions in the crystal considered by (Cochran 1969, Vendik and Zubko 1997). It was rather successfully used in the past for interpretation of dielectric and ferroelectric properties of ferroelectrics. At present there are a number of different approaches (Dawber et al. 2005), and among them the density function theory is the most powerful (Chosez and Junquera 2006), which, with the advances of computers, will enable to solve such a complex problem as synthesis of ferroelectrics with the desired properties. Here the main features of the dynamic theory will be considered. It does not result completely correct temperature and frequency dependences of the dielectric properties. However, it helps to understand the essence of the dynamic theory and introduce the "soft" mode frequency, often used in the dynamic theory of the ferroelectrics.

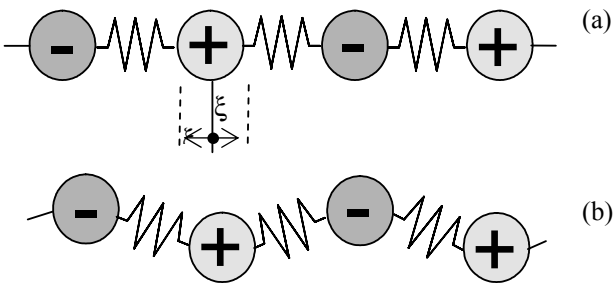

Fig. 2.3.3 Longitudinal (a) and transversal (b) oscillations in a chain of ions

In a simple one dimensional model of an ionic crystal shown in Fig. 2.3.3 the interactions between the ions is represented by mechanical springs allowing propagation of the oscillations along the ionic chain. The ions may oscillate along the chain (longitudinal phonons) and perpendicular to the chain (transverse phonons). In terms of quantum mechanics the thermal oscillations are regarded as phonons characterized by energy hv, where h is the Plank's constant and v is the frequency of the oscillations. The ferroelectric properties of the crystal are explained by instability of thermal oscillations (vibrations) of the ions, i.e. phonons. The motion of the ions is controlled by long range Coulomb interaction forces and inertial (Newton) forces. In contrast to non ferroelectric crystals, to characterize the ferroelectric phase transformation, in a ferroelectric crystal the non-Coulomb (short range) inharmonic interaction forces are also taken into account.

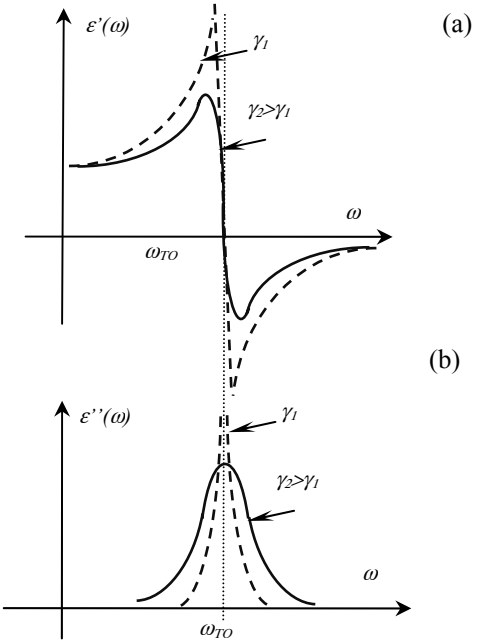

Fig. 2.3.4 Frequency dependencies of the real and imaginary parts of the permittivity following from (2.3.9) for two damping coefficients γ

The complex permittivity may be written as:

$$\varepsilon = \varepsilon_{opt} + \frac{\varepsilon_{DC} - \varepsilon_{opt}}{1 - \left(\frac{\omega}{\omega_{TO}}\right)^2 + j\gamma\left(\frac{\omega}{\omega_{TO}}\right)} \tag{2.3.9}$$

where ε_{DC} and ε_{opt} are permittivity at low, $\omega << \omega_{TO}$, and optical, $\omega >> \omega_{TO}$, frequency limits. Typically $\varepsilon_{opt} << \varepsilon_{DC}$ and ε_{opt} may be ignored at microwave fre-

quencies. It is shown that the frequency of the transverse optical mode, $\omega_{TO} \sim (T - T_c)$, i.e. it goes to zero at phase transition (Curie) temperature. The frequency dispersion of the permittivity given in (2.3.9) is known as dumped resonance dispersion, where γ is the damping coefficient. The frequency dependences of the real and imaginary parts of the permittivity corresponding to (2.3.9) are shown in Fig. 2.3.4. With no damping, i.e. $\gamma=0$, the real part of the permittivity $\varepsilon' \to 0$ at $\omega=\omega_{TO}$. At very low frequencies (for $SrTiO_3$ f< 0.5–1.0 THz) the real part of the permittivity is constant. At frequency $\omega=\omega_{TO}$, known as the "soft" mode frequency, the real part of the permittivity is zero (Fig. 2.3.4 (a)). With increasing damping, $\gamma_2 > \gamma_1$, the resonant feature (increase in real part of permittivity, Fig. 2.3.4 (a)) disappears and the dispersion of the permittivity, below ω_{TO}, similar to Debye relaxation.

When the forces (destabilizing the symmetric phase) in the unit cell of a dielectric crystal tend to displace a ferroelectrically active ion (i.e. *Ti* in $BaTiO_3$) from its position of symmetry it is said the crystal becomes instable. In other words the forces lead to appearance of a dipole moment in the unit cell. At the same time the crystal tends to stabilize its symmetric phase, which causes fluctuations of the ferroelectrically active ions about their equilibrium positions. In the case these fluctuations result in dynamic stabilization of the symmetric phase the crystal is said to be virtual (incipient) or quantum paraelectric. They do not stabilize in ferroelectric-polar phase at any temperature. There are only a few quantum paraelectrics (Lemanov et al. 1999): $SrTiO_3$, $CaTiO_3$, $KTaO_3$, TiO_3 etc. On the other hand the polar ferroelectric phase in these (incipient ferroelectric) crystals may be induced/stabilized by extra external forces like strain (Haeni et al. 2004) and electric field (Hemberger et al. 1995). In some crystals the destabilizing (the symmetric phase) are so strong that they do not undergo paraelectric phase transitions up to the melting point. These crystals are said to be pyroelectrics.

2.4 Engineering Models of the Dielectric Permittivity

2.4.1 Barrett's Formula. Bulk Single Crystals

The first useful formula for temperature dependence of the permittivity was proposed by Barrett (Barrett 1952):

$$\varepsilon = A + \frac{C}{(T_1/2)\coth\left[(T_1/2T) - T_o\right]} \tag{2.4.1}$$

For perovskites, known as quantum paraelectrics or incipient ferroelectrics, the parameters involved in the above formula are given in Table 2.4.1 (Lemanov et al. 1999).

Table 2.4.1 Parameters of Barett's model for incipient ferroelectrics

	ε(300K)	ε(0K)	A	C, 10^4K	T_o, K	T_1,K
$CaTiO_3$	168	331	43.9	4.77	–111	110
$SrTiO_3$	305	20 000		8	35.5	80
$KTaO_3$	239	3840	47.7	5.45	13.1	56.9
TiO_2	170	257				

2.4.2 Rupprecht–Bell–Silverman Model. Bulk Single Crystals

Later, based on the experimental results, Rupprecht et al. (1961) proposed an empirical formula for the temperature and DC electric field dependent permittivity for STO:

$$\varepsilon(E,T)=\frac{\varepsilon(0,T)}{1+(A_{hkl}/C)\varepsilon^3(0,T)E^2}, \tag{2.4.2}$$

where the temperature dependent permittivity at zero bias field is given by (2.3.6):

$$\varepsilon(0,T)=\frac{C}{T-T_c} \tag{2.4.3}$$

(2.4.2) is valid for temperature range 90–230 K and is essentially the same as (2.3.8) where the experimentally defined coefficients A characterize the anisotropic static nonlinearity:

$$A_{100}=1.15\cdot10^{-18}, \quad Km^2/V^2$$
$$A_{110}=0.96\cdot10^{-18}, \quad Km^2/V^2$$
$$A_{111}=0.69\cdot10^{-18}, \quad Km^2/V^2$$

These anisotropic nonlinearity constants are frequency and temperature independent, but have noticeable dependences upon the orientation of the applied external electric field E with respect to crystallographic axes. These formulae predict some anisotropy above structural phase transition temperature 110 K, indicating the slight deviation from ideal cubic structure, observed at room temperature becomes enhanced with the reducing temperature and leads to cubic-to-tetragonal structural phase transition. Similar anisotropy in single crystal STO above phase transition temperature 110 K is observed in other experiments (Eriksson et al. 2003). As it is shown below, this anisotropy has a stronger impact on the loss tangent.

2.4.3 Vendik's Model. Bulk Single Crystals

A phenomenological model for the DC filed and temperature dependent permittivity, for paraelectric phase $B_xSr_{1-x}TiO_3$, proposed by Vendik and Zubko (2000); takes into account also the defects in the crystal:

$$\varepsilon(E,T)=\frac{\varepsilon_{oo}}{\left\{\left[\xi(E)^2+\eta(T)^3\right]^{0.5}+\xi(E)\right\}^{2/3}+\left\{\left[\xi(E)^2+\eta(T)^3\right]^{0.5}-\xi(E)\right\}^{2/3}-\eta(T)}, \quad (2.4.4)$$

where

$$\xi(E)=\sqrt{(E/E_N)^2+\xi_s^2}$$

$$\eta(T)=\sqrt{(\Theta/4T_c)^2+(T/T_c)^2}-1$$

$$E_N=2D_N/\left|\varepsilon_o(3\varepsilon_{oo})^{3/2}\right|$$

D_N=4.2 C/m^2. The involved in the above expressions parameters for $B_xSr_{1-x}TiO_3$, $SrTiO_3$ and $KTaO_3$ are given in Table 2.4.2 (Vendik et al. 2002).

Table 2.4.2 Modal parameters for $B_xSr_{1-x}TiO_3$ (x<0.5)

	$SrTiO_3$	$B_xSr_{1-x}TiO_3$	$KTaO_3$
T_c, K	42	$T_c(x)= 42+439.37x–95.95x^2$	32.5
C	0.86	$C(x)= (0.86+1.1x^2)10^5$	$0.45\cdot10^5$
Θ, K	175	175	170
$\varepsilon_{oo}(x)$	2080	$= C(x)/T_c(x)$	1390
$E_N(x)$, kV/cm	19	$E_N(x)=8.4/\{\varepsilon_o[3\varepsilon_{oo}(x)]^{3/2}\}$	15.6
ξ_s	0.18	0.3	0.02

The defects induce local fields and cause statistical dispersion of the external DC bias field. The local fields may be associated with the residual polar phases and/or charged defects. In oxides, including the perovskites, the oxygen vacancies are the most common positively charged defects. They induce local mechanical strain and electric field around them.

Not only charged, but also neutral defects may cause local polar phases and associated local fields in single crystal paraelectrics. The parameter $\xi(E)$ in the above formulas takes into account these effects via statistical averaging of the applied DC and local electric fields.

Notice once more, that the above formulae are valid for paraelectric phase, where $\xi(E)^2+\eta(T)^3>0$. It is shown in (Vendik and Zubko 2000) that in a ferroelectric (excluding incipient ferroelectrics) the ferroelectric phase transition T_{ph}, the

Curie temperature T_c, and the temperature of the permittivity maximum, T_m, are related as: $T_{ph} < T_c < T_m$. The temperature dependences of the permittivity of $SrTiO_3$ and $B_{0.5}Sr_{0.5}TiO_3$ computed using the above expression (2.4.4) is shown in Fig. 2.4.1.

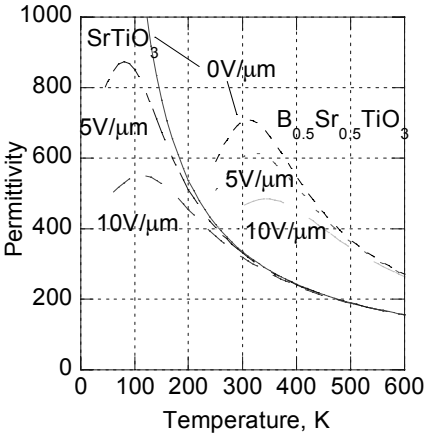

Fig. 2.4.1 Permittivity vs. temperature for at DC bias fields 0, 5 V/μm/ and 10 V/μm

2.4.4 Granular Ceramics and Composites

Ceramic ferroelectrics consist of nanometer-micrometer sized and tightly packed grains. Typically the surfaces/interface layers of the grains have different than the cores of the grains dielectric properties. For the modeling purposes the structure of the ceramics (bulk, thick or thin film) used in tunable microwave devices is represented by simplified models (Fig. 2.4.2). The simple single phase ceramics consist of tightly packed nano or micro sized ferroelectric grains (Fig. 2.4.2 (a)) and columns (Fig. 2.4.2 (d)), perhaps with some ferroelectrically active or passive ("dead layer") grain boundaries. The ceramic composites may consist of the grains of more than one ferroelectric composition (or/and phase) and may contain non-ferroelectric grains (Fig. 2.4.2). The thin films may have composite layered structure (Fig. 2.4.2 (c)), columnar ceramic (Fig. 2.4.2 (d)), and composite columnar (Fig. 2.4.2 (e)) structure. Figure 2.4.3 shows an experimental example of how adding a non-ferroelectric MgO transforms $Ba_{0.8}Sr_{0.2}TiO_3$ from simple ceramics to doped and finally to composite ceramic structure (Su and Button 2004). The models of simple granular ceramics (with grain boundaries) and composite ceramics have been considered in the past (Tagantsev et al. 2005). The analysis of the reported performances show that the microwave performances (loss tangent, tuneability) of the granular ceramics (thin, thick film, bulk) are not as good as the performances of the single crystals and columnar epitaxial films.

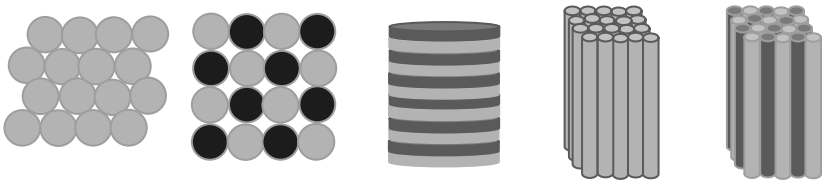

Fig. 2.4.2 Models of ceramics: (a) granular single phase, (b) granular composite, (c) layered composite, (d) columnar single phase, and (e) columnar composite

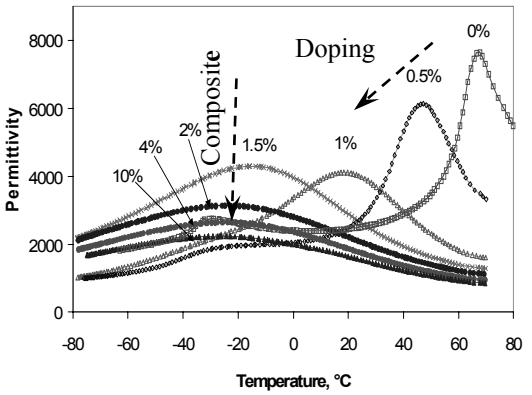

Fig. 2.4.3 The effect of *MgO* on permittivity of $Ba_{0.8}Sr_{0.2}TiO_3$ (Courtesy of T. Button, University of Birmingham, UK)

The apparent permittivity of two-phase composite layered, Fig. 2.4.2 (c), and columnar, Fig. 2.4.2 (e), are given by:

$$\varepsilon_{ap} = \frac{\varepsilon_1 \varepsilon_2}{p\varepsilon_2 + (1-p)\varepsilon_1} \tag{2.4.5}$$

$$\varepsilon_{ap} = q\varepsilon_1 + (1-q)\varepsilon_2 \tag{2.4.6}$$

In these expressions $p=t_1/(t_1+ t_2)$ and $q=A_1/(A_1+ A_2)$ are the relative content (concentrations) of the phases, where t_1 and t_2 are the thicknesses of the phases 1 and 2 (Fig. 2.4.2 (c)), while A_1 and A_2 are the areas of the two phases (Fig. 2.4.2 (e)). In general one of the phases may be passive, i.e. non-ferroelectric. In the case of single phase ceramics the interfacial/inter-columnar non-ferroelectric ("dead") layers may be considered as one of the phases appearing in (2.4.5) and (2.4.6).

2.4.5 Columnar Thin Film Ceramics and Composites

In contrast to granular ceramics, the performance of the columnar films (losses, tuneability etc.), especially in parallel-plate varactors, is close to the single crystals.

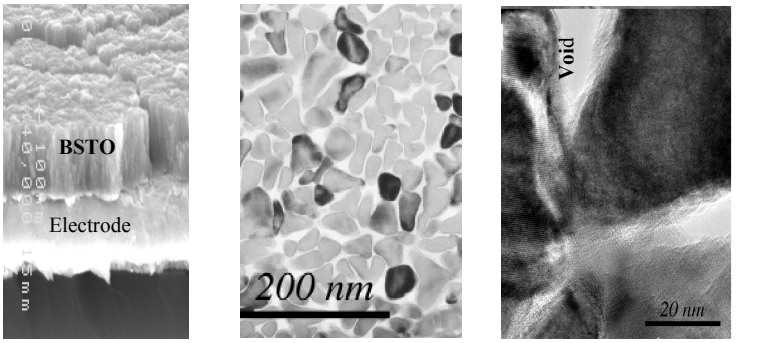

Fig. 2.4.4 Cross-sectional SEM (a) and in-plane TEM (b, c) images of a laser ablated $Ba_{0.25}Sr_{0.75}TiO_3$ film

The cross-sectional scanning electron microscope (SEM) photo (Fig. 2.4.4 (a)), and in-plane transmission electron microscope (TEM, Fig. 2.4.4 (b) and (c)), images of a columnar BSTO film are shown in Fig. 2.4.4. The column boundaries are amorphous, and in some cases contain voids (Fig. 2.4.4 (c)). A distorted region near the electrode/ferroelectric interface at the bottom electrode and amorphous regions at the grain/column boundaries are clearly seen. The analysis of the microstructure and the C-V performance shows that the interfacial distorted layer is about 50–100 nm thick and it is strained.

Figure 2.4.5 represents a simplified model of the columnar film. Each nanocolumn consists of single crystal core, column boundaries, and an electrode/ferroelectric interface layer. Typically the interfacial layer has lower permittivity due to the dislocations, strain, etc. The grain boundaries play a substantial role both in dielectric properties and reliability of the devices based on ferroelectric varactors.

The lower permittivity and tuneability in paraelectric films, in comparison with the bulk single crystal and ceramics of the same composition, have been attributed to the stresses, “dead” layers at the interfaces with the electrodes, non-stoichiometry, voids in the granular/columnar structure, etc. Besides, there are also fundamental effects associated with the surfaces/interfaces. For example, the near surface layer of pure bulk single crystal STO, (which has no ferroelectric phase at any temperature), undergoes a structural phase transition (ferroelectric phase) at about 45 K above the structural phase transition (at about 110K) of bulk single crystal STO (Mishina et al. 2000). With decreasing the film thickness, the contribution of the interface properties increases, relative to the bulk properties and, in nano-size limits, may dominate over the bulk properties.

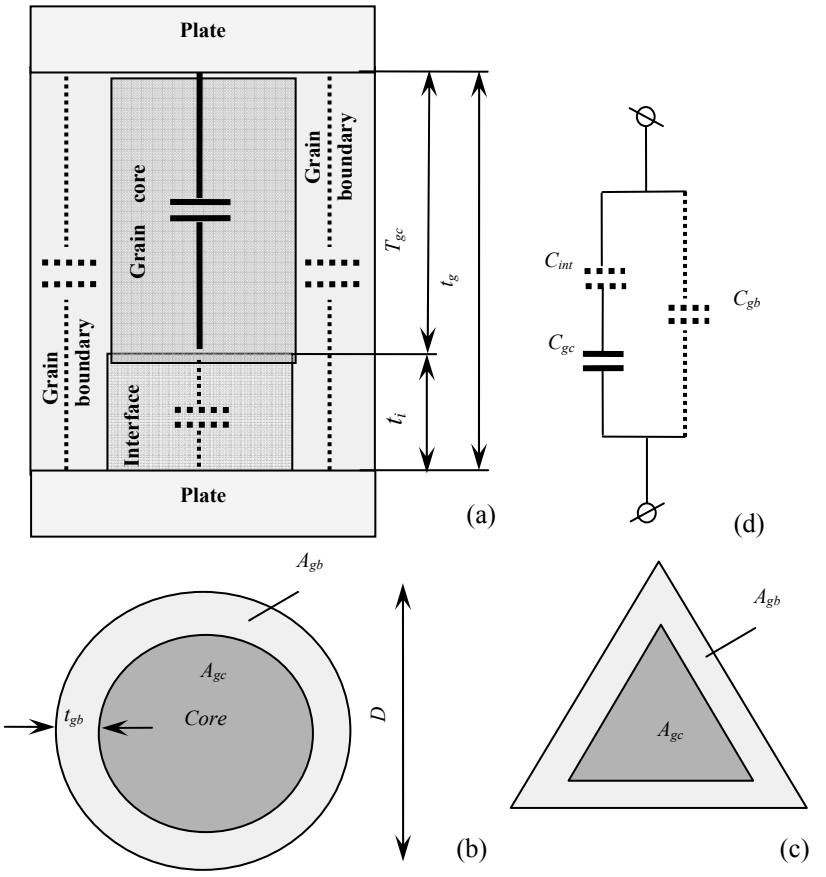

Fig. 2.4.5 Simplified out-of plane (a) and in-plane (b, c) cross sections of a ferroelectric column in a parallel-plate varactor, and its equivalent circuit (d). Reprinted with permission from Wiley©2008

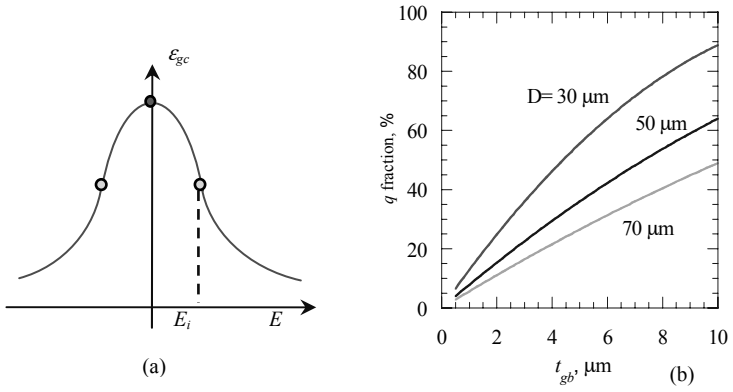

Fig. 2.4.6 C-V of the core with the inflection point (a) and fraction q vs. thickness of the grain boundary for circular shaped cylindrical column. Reprinted with permission from Wiley©2008

The in-plane cross section of the predominantly cylindrical nano-columns (Fig. 2.4.4 (a)) may be modeled by circular (Fig. 2.4.5 (b)), or triangular (Fig. 2.4.5 (c)) shapes. In general, all three regions of the nanograin (Fig. 2.4.5 (a)) may have different properties (due to stress, compositions etc.), and they experience different changes under the applied to the plates voltage. The integral change in the capacitance under the applied electric field is a result of changes taking place in all three parts of the nano-column. These parts of the nano-column may be represented by equivalent capacitances, as shown in Fig. 2.4.5 (d). Then the capacitance of the grain is $C(E,T)=\varepsilon_{ap}\varepsilon_0 A_g/t_g$, with ε_{ap} being the apparent (measured) permittivity defined as:

$$\varepsilon_{ap} = q\varepsilon_{gb} + (1-q)\frac{\varepsilon_{\text{int}}\varepsilon_{gc}}{p\varepsilon_{gc} + (1-p)\varepsilon_{\text{int}}} \tag{2.4.7}$$

$q=A_{gb}/A_g$, $p=t_{int}/_g$, *where* $A_g=(A_{gc}+A_{gb})$ and $t_g=t_{gc}+t_{int}$, A_{gc}, and A_{gb} are correspondingly the areas of the grain core and boundary, t_{gc} and t_{int} are correspondingly the thickness of the grain core and interfacial layer (Fig. 2.4.5). The first term in (2.4.7) is due to the grain boundary, while the second term is due to grain core and interface. In this simplified model the grain boundaries and the interface layer of the films are assumed to have DC field independent permittivity, ε_{gb} and ε_{int}. The apparent permittivity (2.4.7) may be rewritten in a simpler form:

$$\varepsilon_{ap} = q\varepsilon_{gb} + (1-q)\varepsilon_{eff} \tag{2.4.8}$$

where ε_{eff} is the effective permittivity of the layered column ("composite") consisting of a grain core (ε_{gc}) and interface (ε_{int}):

$$\varepsilon_{eff} = \frac{\varepsilon_{\text{int}}\varepsilon_{gc}}{p\varepsilon_{gc} + (1-p)\varepsilon_{\text{int}}} \tag{2.4.9}$$

An analytic expression for ε_{eff} may be found in (Tagantsev et al. 2005). An alternative approach, given here, is based on (2.3.8) and modified Curie-Weiss low (Rupprecht and Bell 1964) representing the zero bias temperature dependence of the permittivity in bulk single crystals as:

$$\varepsilon_{gc}(0,T) = \varepsilon_L + \frac{C_k}{T-T_c} \tag{2.4.10}$$

where the temperature independent term ε_L is the background permittivity, i.e. the permittivity at very high ("infinite") temperature where there is no soft mode contribution. The extrapolation, using (2.4.10), gives ε_L in the range 39–58 for typical perovskites like $BaTiO_3$, $SrTiO_3$, $CaTiO_3$, $KTaO_3$ (Rupprecht and Bell

1964). However this extrapolation seems questionable sine it is based on the soft mode permittivity whereas the permittivity of the crystal at extremely high temperatures may be associated with other phonons. Typically ε_L is assumed to be about 7–8 (Noeth et al. 2007). For applied DC voltage V the electric field developed in ferroelectrically active core of the column is:

$$E_{gc} = \frac{\varepsilon_{\text{int}}(1-p)}{\varepsilon_{gc}p + \varepsilon_{\text{int}}(1-p)}\frac{V}{t_{gc}} \tag{2.4.11}$$

where ε_{gb} and ε_{int} are DC bias and temperature independent. The temperature and the DC bias dependences of ε_{gc} are given by (2.4.10) and (2.3.8). Finally, the apparent permittivity of the film is:

$$\varepsilon_{ap}(E,T) = q\varepsilon_{gb} + (1-q)\frac{\varepsilon_{gc}(0,T)}{1+\frac{1}{3}\left(\frac{E_{gc}}{E_i(T)}\right)^2}, \tag{2.4.12}$$

where $E_i(T)$ is the field corresponding to the inflection point in the C-V dependence of the bulk single crystal (Fig. 2.4.6 (a)):

$$E_i = \frac{1}{3\sqrt{\beta\left[\varepsilon_o\varepsilon_{gc}(0,T)\right]^3}} \tag{2.4.13}$$

(2.4.13) is easy to deduce by taking the second derivative of (2.3.8) vs. field. The nonlinearity coefficient β itself is temperature dependent. For $SrTiO_3$ $\beta \approx 8\cdot 10^9$ JC^{-4} m^{-5} at room temperature. (2.4.12) may be used to develop scalable field and temperature dependent capacitance of parallel-plate varactors. Required for modeling parameters: p, q, ε_{gb} and ε_{int}, C_k, T_c, ε_L, β, T and V, where p, q, ε_{gb} and ε_{int}, are ferroelectric film (fabrication method) specific-available from experiments, while C_k, T_c, ε_L, β are fundamental parameters for the given ferroelectric.

2.5 Models of the Loss Tangent

2.5.1 Loss Mechanisms and Early Models of the Loss Tangent

In the past, loss has been a major problem hindering the commercialization of tunable microwave devices based on ferroelectrics. Although recently a considerable progress has been achieved, especially in thin film ferroelectrics, the problem of loss is still an issue for some demanding applications, and needs further theoretical

and experimental treatments. In this section the main loss mechanisms are considered briefly. Ferroelectrics in only paraelectric phase are considered. A rather comprehensive overview of the losses in microwave ferroelectrics is given by Tagantsev etc. (Tagantsev et al. 2005). There are two major groups of microwave losses in paraelectric phase ferroelectric; intrinsic and extrinsic (Fig. 2.5.1). In a perfect, single crystal paraelectric, the dissipation (losses) of the microwave power is associated with the absorption of the (microwave) electromagnetic waves by the thermal oscillations of the ions, and by the free charge carriers. In ideal single crystals ferroelectric (e.g. $SrTiO_3$, $KaTaO_3$, $Ba_xSr_{1-x}TiO_3$ etc.) without defects, used in tunable microwave devices, these fundamental-intrinsic losses are typically very small and may not be eliminated or reduced. These losses define the minimum value of the loss tangent which a given paraelectric may have. In real crystals, and especially in thin films, the dissipation of the microwave energy is associated with the defects and may be much higher. These are externally imposed losses and may be reduced or, in an ideal case, eliminate by synthesis of crystals with the reduced defect density. They are especially high in ceramics and thin ferroelectric films. The reduction of the defect density, especially in thin epitaxial films used in integrated tunable microwave devices, was and remains a challenging problem.

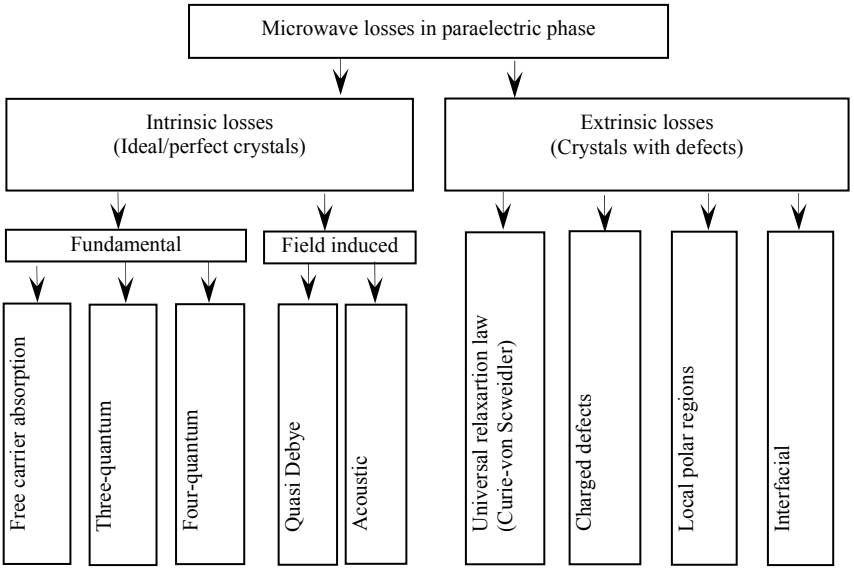

Fig. 2.5.1 Brief classification of the loss mechanisms in paraelectrics

Both the theoretical and experimental study of the loss in ferroelectrics is a more complex problem that that of the permittivity. In the past, a systematic experimental study of the dielectric properties, and particularly the losses has been carried out by (Bete 1970), (Rupprecht and Bell 1962) etc.

Rupprecht–Bell–Silverman model of the nonlinear loss tangent, which is based on experiments using single bulk crystal STO, reads:

$$\tan\delta = \tan\delta_o + \tan\delta_F \tag{2.5.1}$$

The field dependent part of it:

$$\tan\delta_F = \omega(B_{kkl}/C)\varepsilon^5(T,0)E^2 \tag{2.5.2}$$

The anisotropic nonlinearity constants are field, frequency and temperature independent. For (100)STO $B_{100} = 4.8\cdot10^{-7}$, Km^2s/V^2. The empirical formula for the temperature dependent term

$$\tan\delta_o = \left\lfloor \alpha + \beta T + \gamma T^2 \right\rfloor / (T - T_C) \tag{2.5.3}$$

For a single crystal STO α=0, β=6.53·10^{-4}, γ=2.54·10$^{-6}K^{-1}$.

Vendik's (1998) model is theoretical, based on four quantum mechanism, and predicts qualitatively correct frequency, temperature and permittivity dependence for the loss tangent discussed below. However, the electric field dependence predicted by this model does not explain the experimentally observed increase in the loss tangent in single crystal paraelectrics STO and KTO. This field dependent loss tangent explained by quasi-Debye mechanism considered in the next section.

2.5.2 Models of the Main Loss Mechanisms

Regardless the mechanisms, the losses, in general, are additive, i.e. the total loss tangent of a paraelectric crystal is a sum of the loss tangents of all involved mechanisms: $\tan\delta = \sum_i \tan\delta_i$, where i denote the loss of a specific loss mechanism, partly discussed below and indicated in Fig. 2.5.1.

Intrinsic Losses

The ferroelectrics used as tunable dielectrics are typically good dielectrics with extremely small density of the free electrons and holes. The mobility of these carriers is also small. Hence the losses associated with the absorption of the electromagnetic energy by the free charge carriers may be ignored in most of the cases (Gevorgian et al. 1997). The fundamental losses are associated with the interactions of the electromagnetic (microwave) energy with the thermal oscillations (phonons hv, h is the Plank's constant, v is the oscillation frequency) of the ions. Most of the following discussions are based on (Tagantsev et al. 2005).

In homogeneous perfect bulk single crystal paraelectrics, such as displacive ferroelectrics with a center-symmetric cubic crystal structure (e.g. $SrTiO_3$, $KaTaO_3$, $Ba_xSr_{1-x}TiO_3$ etc.) the fundamental losses are associated with the interac-

tions of the microwave field with the phonons. The loss tangent deduced from simple damped resonance (dispersion) model gives the following temperature and frequency dependences: $tan\delta \sim \omega\varepsilon T$, which, due to used simplifications and assumptions, does not reflect the experimentally observed slopes of the temperature $\varepsilon(T)$ and frequency $\varepsilon(\omega)$ dependences.

Microwave energy is absorbed by thermal phonons of the crystal and the dissipated energy heats the crystal. In fact, the energy of phonons, hv, in the crystal is much higher then the quantum hf of the microwave field, $hv > hf$. Here f is the frequency of microwave field. In terms of quantum mechanics the absorption takes place via three and four quantum mechanism. In the first case the absorption process involves one microwave quantum hf and two phonons. In microwave and millimeter wave and near room temperature regions this theory predicts the following frequency and temperature dependence:

$$\tan\delta_{ph} \propto \omega\varepsilon^{3/2}T^2 \tag{2.5.4}$$

ε is the relative permittivity of the ferroelectric.

In the case of four-quantum process one microwave quantum hf interacts (dissipated) with three phonons of the crystal. In the same temperature and frequency regions this theory predicts frequency and temperature dependences of loss tangent similar to three-quantum one (2.5.4). However, for the typical paraelectrics (BTO, STO), KTO) the three quantum dissipation is dominant. The four phonon mechanism is applicable to crystals with non-center symmetric structure, e.g. ferroelectrics in polar phase.

In perfect crystals, besides the fundamental phonon losses discussed above, extra microwave losses appear due to free charge carries and under the external electric field. The external fields, both DC, and even high power microwave fields break the symmetry of the crystal structure of the paraelectric phase by virtue of electrostrictive effect. In a crystal with a symmetric lattice structure (i.e. cubic as in $SrTiO_3$, $KaTaO_3$, and in paraelectric phase $Ba_xSr_{1-x}TiO_3$) the external field shifts the centers of the positive and negative charges. The induced non-center symmetric unit cell of the crystal lattice becomes polarized with an external field dependent dipole moment. The microwave field experiences microwave losses typical to actual non-center symmetric crystals, although the crystal is still in paraelectric phase. In an extreme case the external DC field may cause paraelectric to ferroelectric phase transformation (Hamburger et al. 1996), resulting in a rapid increase of microwave losses.

The induced electric dipole initiates two extra mechanisms of the microwave losses: i) DC filed induced Quasi-Debye, and ii) Microwave to acoustic transformations. The field induced Quasi-Debye mechanism is proposed by Tagantsev (Tagantsev et al. 2005) and for small tuneability ($T(E)=((\varepsilon(0)-\varepsilon(E))/\varepsilon(E)) << 1$) the losses associated with this mechanism are characterized by the following functional dependences of the loss tangent on the frequency and electric field:

$$\tan\delta_{QD} = AI(E)\omega T(E) \tag{2.5.5}$$

where *T(E)* is the tuneability of the dielectric permittivity:

$$T(E) = \frac{\varepsilon(0) - \varepsilon(E)}{\varepsilon(0)} \tag{2.5.6}$$

A is a material related constant. Experimental values of *A* for single crystal STO and KTO are accordingly $23 \cdot 10^{-3}$/GHz and $17 \cdot 10^{-3}$/GHz, $I(E) \approx 1$ for small tuneability, $T(E) << 1$. For small tuneability, using (2.3.8), (2.5.4) may be reduced to:

$$\tan \delta_{QD} = 3A\beta \left[\varepsilon_o \varepsilon(E)\right]^3 \omega E^2 \tag{2.5.7}$$

i.e. the functional dependence on *E* and ω coincide with (2.5.2). The parabolic dependence of $tan\delta_{QD}$ measured at about 0.8 GHz at 40 K, for a bulk single crystal [100] STO (Eriksson et al. 2003), is shown in Fig. 2.5.2. The maximum applied DC field is 1.0 V/μm. At fields below about 0.2 V/μm [$T(0.2V/\mu m) < 0.1$] the dependence is to larger degree parabolic. However, at about 0.5 V/μm the losses reach maximum and start reducing slightly, as predicted by Quasi-Debye mechanism at high electric field (and larger tuneability, Astafiev et al. 2005). In thin $SrTiO_3$ films devices the applied fields are typically much higher, up to 100 V/μm and above. Hence this loss mechanism should result in slight reduction of the losses, at least above 10.0 V/μm. For *Ba* reach compositions the field dependence of the Quasi-Debye losses is weaker.

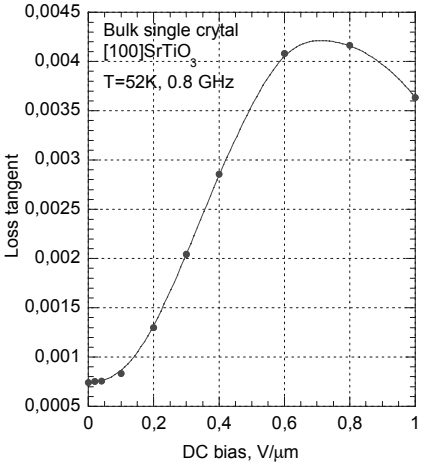

Fig. 2.5.2 DC field dependence of the loss tangent of [100] STO at 52 K and about 0.8 GHz

The electric field induced microwave to acoustic transformations in a homogeneous bulk single crystal paraelectric is associated with the electrostriction and inverse piezoelectric effects. Due to these two effects the electromagnetic field

generates acoustic waves with the same frequency as the microwave signal itself. In a non-ferroelectric piezoelectric (i.e. Quartz) the amplitude of the acoustic waves generated by electrostriction is proportional to E^2, while the converse piezoeffect generates acoustic waves with amplitudes proportional to E. However, in a paraelectric with induced dipole moment this dependence is more complex, since the dipole moment itself depends on the applied DC field. In homogeneous paraelectric crystals the losses of the microwave energy are associated with the attenuation of the acoustic waves. In a crystal with a limited sizes (e.g. by electrodes) the acoustic waves may additionally attenuated in the interfacing materials. On the other hand, the limited sizes of the crystal may cause reflections resulting in acoustic waves resonances and resonant absorption (peaks in loss tangent) of the microwave energy. Typically, the resonant peaks in loss tangent associated with the acoustic resonances are visible in experiments where the density of the defects is very low and the extrinsic losses are smaller. In crystals much larger than the acoustic wavelength (i.e. in STO disk resonator (Eriksson et al. 2003) these resonances may form a quasi-continuous spectrum. In thin films a clear discrete spectrum is observed (Gevorgian et al. 2006). The losses in resonant absorption should increase linearly or quadratic with the increasing external DC field depredating on the relative contributions of the induced piezoelectric and/or electrostriction effects. In general, the field induced transformations of microwaves into acoustic waves are negative for analog tunable microwave devices. On the other hand this effect may be utilized in DC field tunable TFBARs (Berge et al. 2008).

Typically, especially in thin films, all intrinsic losses are "screened" by higher contributions from extrinsic losses discussed below. However, in high quality bulk, and recently in epitaxial films, the intrinsic and extrinsic losses appear to be comparable. With decreasing the density of the defects the intrinsic losses start dominating. In an ideal paraelectrics crystal without defects, where all extrinsic losses are removed, the electric field induced quasi-Debye losses and the losses associated with the microwave to acoustic transformations will limit the achievable minimum losses.

Extrinsic Losses

In crystals with defects there are extra losses associated with the defects in the crystal structure. The extrinsic losses are the main trouble makers, and they are much higher then the intrinsic losses. However, in contrast to the intrinsic losses, these losses may be reduced by reducing the density of the defects. Given below is a brief overview of the main loss mechanisms, caused by defects.

Universal (Curie-von-Schweidler) relaxation mechanism is the most common defect related mechanism for all dielectrics in general, including paraelectrics.

$$\tan \delta_{ur} = R\omega^n \tag{2.5.8}$$

n=0–1 depredating on the material nature of the defects in it.

Charged defects are one of the most common defects. Both in chemically pure bulk single crystals, ceramics and thin films ferroelectrics any charged point defects and charged dislocations create local static electric field. Even the neutral defects may locally distort the crystal symmetry and create local dipoles and static fields around them. The oxygen vacancies seem to be the most common positively charged point defects in chemically pure crystals. In such local felid both electrostrictive (Vendik and Platonova 1971) and converse piezoelectric effects are active and the electromagnetic (microwave) waves generate acoustic waves. From these point sources (in contrast with the defectless case discussed above) the acoustic waves travel in the crystal taking with them some energy from the electromagnetic waves, i.e. causing loss of the microwave signal. Some local increase in the loss tangent also may be expected by virtue of the quasi-Debye mechanism. The loss tangent associated with the charged defects is approximated by:

$$\tan\delta_{ch} = F\varepsilon\omega\frac{Z^2 n}{4\pi\rho v_t^3}\left\{1-\frac{1}{\left[1+(\omega/\omega_c)^2\right]^2}\right\}, \tag{2.5.9}$$

where $F\approx 1$ is a material specific constant, Z the effective charge (C) of the defect, n is the density (m^{-3})of the defects, ρ is the density of the crystal (kg/m^3), v_t is the acoustic velocity, $\omega_c=v_t/r_c$, r_c is the correlation length of the charge distribution, i.e. the distance at which the electro-neutrality in the crystal is restored. As it follows from (2.5.8) the loss tangent in this case is proportional to the permittivity, indicating that it follows the same temperature and field dependences. For a paraelectric this means a reduction of the losses with increased field and temperature. The charged defects may be uniformly distributed in the bulk of the crystal and/or concentrated at the interfaces with the grains and electrodes. Recent publications indicate that oxygen vacancies are the main charged defects and, in some cases, the main contributors to the losses in thin ferroelectric films.

Notice that in contrast to external DC field induced microwave and acoustic transformations considered above as a part of the intrinsic losses, the losses in this case associated solely with the defects, i.e. they have extrinsic nature, and may be reduced by eliminating the defects. On the other hand the losses associated with the external filed induced acoustic transformation in perfect, defectless crystal are more of intrinsic nature. They are “hidden” in the perfect crystal, and appear as soon as an external field is applied. Under an applied DC bias both these intrinsic and extrinsic losses contribute in the total losses of a tunable ferroelectric device. After removing the external field, only the extrinsic part associated with the charged defects contribute.

Other Sources of Extrinsic Losses: Local polar regions occur in normally paraelectrics (Hubert et al. 1997) at the interfaces between the phases, grains/ columns, electrodes and other layers (i.e. dielectric and metallic buffer layers). No reports are available on the losses associated with these defects.

In paraelectric phase single crystals (e.g. $SrTiO_3$, $KTaO_3$ etc.) the quasi-Debye mechanism (2.5.7) dominates, as it is seen from the experimental result shown in Fig. 2.5.2. It is characterized by linear frequency dependence and a field dependence which at low field strengths may be approximated by a quadratics function (2.5.2). The temperature dependence is similar to the temperature dependence of the permittivity as in (2.5.7). One expects to have similar frequency, field and temperature dependences in high quality defect free thin films. However, the experiments reported until now indicate that the losses in the thin films increase linearly with the frequency and decrease with the electric field as it is predicted by (2.5.9), i.e. it seems the losses associated with the charged defects dominate. At the same time the losses in the reported paraelectric phase decrease with the increasing temperature, as one also expects from the temperature dependent permittivity in (2.5.9).

2.6 Dielectric Nonlinearities

2.6.1 Nonlinear Performance of Paraelectrics

Ferroelectrics are essentially nonlinear materials. In some applications (i.e. harmonic generators, pulse compressors, limiters) the nonlinearity is a desired effect, however, in most of the applications nonlinearities cause serious problems such as harmonic generation and intermodulation distortion (known as IP3).

When considering nonlinearities one has to distinguish between the static and dynamic nonlinearities. The static nonlinearity appears in DC dependent permittivity and microwave losses tangent. In this case the level of the microwave probe signal is low and does not cause any measurable nonlinearity. The dynamic nonlinearity is characterized by substantial dependence of the permittivity and loss tangent on the level of the RF/microwave power, even without any applied DC field. Theoretically, for paraelectric phase for $Ba_xSr_{1-x}TiO_3$ and similar ferroelectrics, the dynamic nonlinearity is four times smaller then the static nonlinearity (Tagantsev and Glazunov 1998). The field and temperature dependence of a ferroelectric in paraelectric phase, based on the thermodynamic theory of Landau, may be represented as (2.3.8):

$$\varepsilon(E,T) = \frac{\varepsilon(0,T)}{1 + 3\beta\varepsilon_o^3\varepsilon^3(0,T)E^2}$$

where β is the coefficient of the dielectric nonlinearity, and the temperature dependence of the permittivity is given by Curie-Weiss low (2.3.6):

$$\varepsilon(0,T) = \frac{C}{T - Tc}$$

Under a small electric field, the static (i.e. under DC bias) and the dynamic (Tagantsev and Glazunov 1998) nonlinear coefficients are given by:

$$\beta_{DC} = \frac{\Delta\varepsilon_{DC}}{3\varepsilon_o^3[\varepsilon(0,T)]^4 E_{DC}^2} \tag{2.6.1}$$

$$\beta_{AC} = \frac{4\Delta\varepsilon_{AC}}{3\varepsilon_o^3[\varepsilon(0,T)]^4 E_{AC}^2} \tag{2.6.2}$$

where $\Delta\varepsilon_{DC}=\varepsilon(0)-\varepsilon(E_{DC})$ and $\Delta\varepsilon_{AC}=\varepsilon(0)-\varepsilon(E_{AC})$ E_{AC} is the amplitude of the microwave signal ($E=E_{AC}Cos(\omega t)$). The relative changes in permittivity may be given as:

$$\frac{\Delta\varepsilon_{DC}}{\varepsilon(0,T)} = 3\beta_{DC}\left[\varepsilon_o\varepsilon(0,T)\right]^3 E_{DC}^2 \tag{2.6.3}$$

$$\frac{\Delta\varepsilon_{AC}}{\varepsilon(0,T)} = 3\beta_{AC}\left[\varepsilon_o\varepsilon(0,T)\right]^3 E_{AC}^2 \approx \frac{1}{4}\frac{\Delta\varepsilon_{DC}}{\varepsilon(0,T)} \tag{2.6.4}$$

It follows from the above expressions that at $E_{DC}=E_{AC}$ the microwave signal causes four time smaller changes in the permittivity. In other words the widely speculated concern (which is based on the DC dependent permittivity) about negative effects associated with the nonlinearities seems to not be justified. Moreover, in tunable microwave devices the DC field is much higher then the AC field: $E_{DC}>E_{AC}$, i.e. while designing a ferroelectric varactor/device one may reduce the nonlinear effects by trading the low nonlinearity against the higher tuning voltages.

Apart from appearance of undesirable harmonics in microwave systems, in some passive device applications the transformation of a part of microwave power into the higher order harmonics may be seen as extra loss, i.e. some useful microwave power ”lost” in generated harmonics. Fortunately the dynamic nonlinearity of ferroelectrics is much lower in comparison with the semiconductors and its impact may be effectively reduced by scaling the sizes of the devices and using smart device designs. Some ways of decreasing the nonlinearities and increasing the power handling capabilities are discussed in Sect. 4.7.

2.6.2 Nonlinearity and Power Handling Capability

In general, the power handling capability may be defined as the maximum power level at which the performance parameters of the devices are still in the specified limits. The performance indicators are device/application specific. As a universal criterion one may compare the amplitude of the microwave signal and the applied DC voltage, i.e. The system/device application limit/specify the maximum amplitude of the microwave field, E_{AC}, with respect to the maximum DC field, E_{DC}, i.e. the E_{AC}/E_{DC} ratio the system may tolerate. The E_{AC}/E_{DC} ratio may be limited by tolerated maximum i) heating, ii) power of higher order harmonics and/or

iii) losses. In general, the ferroelectric varactors are characterized with higher than semiconductor analogs power handling capability. In contrast to semiconductor competitors, the ferroelectric devices may be easily scaled to support higher microwave powers by i.e. increasing the thickness of the ferroelectric film in parallel-plate varactors and the gap in coplanar plate varactors. Moreover, the varactors may be cascaded allowing low DC control voltages and at the same time supporting higher microwave powers (see Sect. 4.7).

2.7 Thin Films vs. Bulk

2.7.1 Thin Film vs. Bulk Single Crystal

The simple models considered in previous sections (e.g. (2.3.8)), in general, are valid for the bulk single crystals. They are useful for understanding the physics of the tunable ferroelectric devices, and in many cases, for modeling of the microwave devices with a reasonable accuracy. In single crystal paraelectric phase perovskites, the deviations from ideal cubic structure cause anisotropy in dielectric properties. For example, the bulk single crystal STO has only very slight tetragonality at room temperature and remains in paraelectric phase at all temperatures up to near 0 K (Muller and Burkard 1979). With the decreased temperature the permittivity increases, and below the phase transition temperature 110 K it becomes tetragonal, with clear anisotropy in the dielectric permittivity. The microwave losses undergo similar changes with the reduction of the temperature, and below phase transition temperature become essentially anisotropic. Figure 2.7.1 shows the measured at microwave frequencies anisotropy in the dielectric losses in bulk single crystal STO (Eriksson et al. 2003).

Although chemically the same, the dielectric properties of the thin ferroelectric (epitaxial, textured) films are substantially, sometimes even drastically, different from their bulk counterparts. The experiments with a 75 nm thick free standing single crystal $BaTiO_3$ film, cut from a bulk single crystal, reveal (Saad et al. 2004) that with the ideally symmetric electrodes and with no substrate the dielectric properties of the film are identical with the single crystal. Typically, in the thinner films the lower permittivity and tuneability, in comparison with the bulk single crystal, are attributed to the low permittivity dead layers at the interfaces with the electrodes. The thickness of the dead layer assumed to be of the order of several nanometers (Stengel and Spaldin 2006). Naturally, its effect will be more pronounced for the films that have thicknesses comparable with the thickness of the dead layer. In thin films grown on host substrates and ceramics the misfit strain (mismatch in lattice parameters and thermal expansion), non-stoichiometry, voids in the granular/columnar structure etc., may have drastic effects on the dielectric and acoustic properties of the films. These factors appear in different degrees in the films produced by different laboratories and methods. Besides, there are also fundamental effects associated with the surfaces/interfaces. With decreasing the film thickness, the contribution of the surface properties, relative to the bulk properties increases

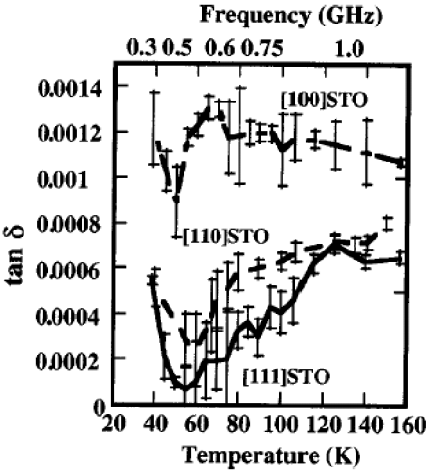

Fig. 2.7.1 Orientation dependent dielectric losses in bulk single crystal STO. Reprinted with permission from AIP©2003

and, in nanostructure limits, may dominate over the bulk properties. The surface of the ferroelectric may have drastically different properties in comparison with the bulk of the crystal. For example, pure bulk single crystal $SrTiO_3$ has no ferroelectric phase at any temperature. On the other hand, a structural/ferroelectric phase transition, at about 155 K is observed in a near surface layer in bulk single crystal STO, (Mishina et al. 2000). Polar gain boundaries in undoped $SrTiO_3$ ceramics are detected by Raman scattering (Petzelt et al. 2001). It is shown, in this work that the polarization is perpendicular to the tetragonal c-axis, and it is temperature independent. This polarization may be associated with the fundamental effects at the interfaces/surface considered above (Mishina et al. 2000), tilted grain boundaries (McGibsson et al. 1996), ad/or charged defects (i.e. oxygen vacancies) at the grain boundaries. Donor type space charge is reported at the grain boundaries (Hagenbeck and Waser 1999). These observations indicate that similar polar phases may be in thin films with granular and columnar structure.

The in-plane anisotropy is even more pronounced in thin the STO and paraelectric phase BSTO films. Under interfacial/misfit strain the lattice of STO and BSTO films are strongly distorted and, in most cases, have tetragonal structure, although being in paraelectric phase. In these films one should expect a substantial anisotropy in the permittivity and microwave losses similar to bulk STO shown in Fig. 2.7.1. Attempts to measure the orientation dependent in-plane anisotropy in the permittivity and losses tangent in strained ferroelectric films have been reported recently. For example, in a parallel plate varactor the films with [110] and [111] orientations are preferable. BSTO films with surface normal orientations (001), (011) and (111) epitaxially grown (001), (011) and (111) oriented *MgO* substrates (Moon et al. 2003) had slight in-plane anisotropy in permittivity. The in-plane Q-factor (=1/$tan\delta$) measured at 9.0 GHz is substantially higher for (111) film. In another experiment (Chang et al. 2005), STO films epitaxially grown on (110)

$DyScO_3$ substrate, measured in plane [100], [010], [110] and [–110] orientations had substantially different permittivity and tuneability in these orientations, largest in in-plane [010] orientation.

The effect of the misfit strain becomes dominant with decreasing the film thickness (grain sizes). In relatively thicker films the strain is released and it has no substantial effect in the bulk of the film, thicker than strain released transition layer. The strain may cause ferroelectric to paraelectric (and vice versa) phase transitions (Pertsev et al. 1998). An extreme case of induced ferroelectric phase transition in strained epitaxial STO film has been demonstrated experimentally (Haeni et al. 2004). Hence, the size associated ferroelectric to paraelectric phase transition is associated with the shift in Curie temperature due to misfit strains. For a given film (composition) the shift depends on the film composition, the difference in the lattice and thermal expansion coefficients between the film and interfacial layers/substrate, the temperature, and the film thickness.

The strong anisotropy in the dielectric losses has to be taken in practical applications of STO, especially in thin film. For example, the gap between the electrodes in coplanar-plate varactors has to be normal to the in plane orientation with the largest tuneability and smallest losses (for example [010], as in (Chang et al. 2005). The films in parallel plate varactors should have [110] and [111] orientation normal to the plates to ensure highest tuneability and smallest losses.

2.7.2 Strain

The strain is defined as a fractional change of the crystal sizes. In terms of the lattice constant, for 1D model, Fig. 2.7.2, it is given as $u=\Delta a/a_o$. The strain in crystals may be caused by changes in:

- Temperature – this corresponds to thermal expansion;
- Mechanical stress – known as elastic deformation;
- External DC field. In this case one has to distinguish between the converse piezoelectric and electrostrictive effects.

Thin films deposited on substrates experience a 2D misfit strain due to the lattice parameter and thermal expansion coefficient differences between the film and substrate. Both of them cause elastic deformations according to i) and ii) above. An extra strain in ferroelectric films used in microwave devices is associated with the applied electric field.

The converse piezoelectric effect may be explained by considering the simple 1D model shown in Fig. 2.7.2, where the interaction forces between the ions are represented by springs. The soft and hard springs represent the different interaction forces between the neighboring ions. In polar phase the external DC field applied to the crystal causes more changes in the length of the soft spring in comparison with the hard spring. As a result the size of the whole unit cell changes, and the change, i.e. the strain is proportional to the external DC field:

$$u = dE \tag{2.7.1}$$

where d is the piezoelectric coefficient, and the strain is an odd function of the applied field E, i.e. the sign of the strain depends on the direction of the external field.

In paraelectric (cubic, center-symmetric) phase, the positive ion is located in the center where its free energy is minimum. In this equilibrium state the springs connecting to the neighboring ions are similar, and the external DC field should not cause strain. In reality, the forces developed between the ions are not linearly related to the external DC field. They are characterized by quadratic dependences with the different spring constants for the left and right springs: $k_1(\Delta a)^2$ and $k_2(\Delta a)^2$. In fact the spring constant is slightly larger when one tries to push the ions closer. This means the crystal is easier to expand than contract (press). The force trying to return the ion into the center equilibrium position is then proportional to the difference $(k_1–k_2)(\Delta a)^2$. This small difference produces a strain which is independent of the direction of the external field:

$$u = gE^2, \tag{2.7.2}$$

where g is the electrostriction coefficient. Notice that the strain in the case of electrostriction is an even function of the applied field, i.e. it does not depend on the direction of the field. This is another feature that may be used to distinguish between the converse piezoelectric and electrostrictive effects. In thin films the thermal, acoustic and electric and electrical properties have mutual coupling. This coupling is discussed in the next section.

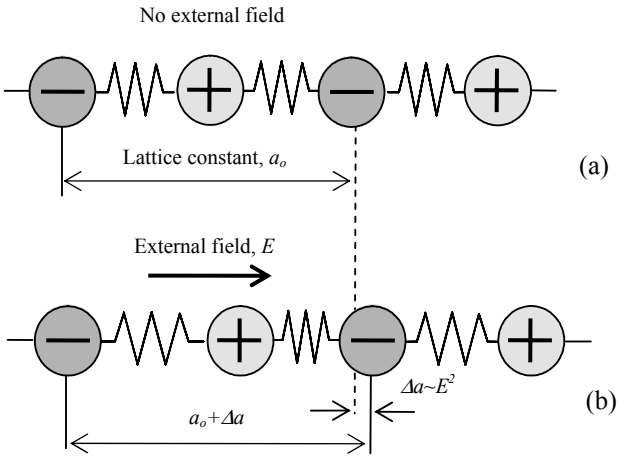

Fig. 2.7.2 1D model of a paraelectric crystal without (a) and with (b) external field

In tunable microwave devices, based on thin film ferroelectrics, the consideration of the electroacoustic properties is of great importance. In tunable devices the films are clamped by substrate, hence they are subject to lattice mismatch and thermal expansion mismatch strains. In contrast to free standing bulk counterparts, these strains generate stresses, which affect dielectric properties of the films, and

may cause large shifts in the Curie temperature and Curie constant, and even result in paraelectric-to-ferroelectric phase transitions (Haeni et al. 2004). Additionally, via electrostriction and inverse piezoelectric effects, induced strains and stresses are generated in the films. The electric filed induced strains are limited in the plane of the film. However, in out of plane orientation, films have freedom for strains. Besides the dielectric properties the acoustic parameters of the film also undergo changes under complex action of misfit and field induced strains. The films, otherwise in paraelectric phase, may take field induced piezoelectric properties. In short, one has to expect substantial differences in both dielectric and acoustic (piezoelectric) properties of the ferroelectric films and their bulk single crystal counterparts. Due to substrate clamping these properties turn to be more interdependent, and while analyzing the film performances and designing devices one has to take these complex interdependences into account.

2.7.3 The Effects of the Strain on Dielectric Properties of the Thin Films

As it was indicated, the properties of the ferroelectrics are sensitive function not only of the electric field and temperature, but also the strain. A thin ferroelectric film clamped by the substrate and other interfacing films experience in plane misfit strain, u_m, associated with the differences in lattice parameters and thermal expansion coefficients of the interfacing layers. The films are free along out of plane direction and are not strained. Under the in-plane strain the lattice of the films undergo certain deformations. For example, normally cubic lattice of a paraelectric film may become tetragonal or orthorhombic, i.e. its symmetricity is reduced. Then the film, though the same chemically, becomes different physically, with the different dielectric and acoustic properties. Particularly the film, otherwise in paraelectric phase, may undergo paraelectric to ferroelectric phase transformation indicated in the previous section.

Figure 2.7.3 shows the conventional axis notations used in the following analysis.

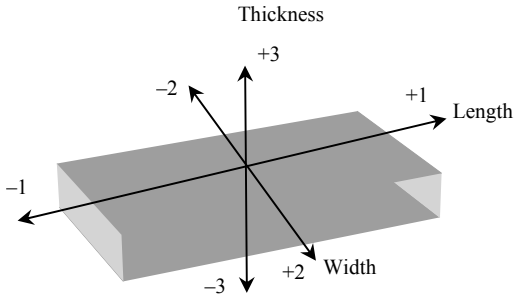

Fig. 2.7.3 Axis notations

The analysis (Tagantsev et al. 2005) shows that, for a film in paraelectric phase (cubic lattice), the in-plane misfit strain caused by an isotropic substrates result in the following in-plane ($\varepsilon_{in}=\varepsilon_{11}=\varepsilon_{22}$) and out-of-plane ($\varepsilon_{out}=\varepsilon_{33}$) permittivities:

$$\varepsilon_{in} = \left\{ \frac{1}{\varepsilon} - 2\varepsilon_o u_m \left[q_{11} + q_{12} - \frac{2\eta}{1-\eta} q_{12} \right] \right\}^{-1} \tag{2.7.3}$$

$$\varepsilon_{out} = \left\{ \frac{1}{\varepsilon} - 2\varepsilon_o u_m \left[2q_{12} - \frac{2\eta}{1-\eta} q_{11} \right] \right\}^{-1} \tag{2.7.4}$$

where ε is the unstrained permittivity of the film which practically is the same as the permittivity of the bulk single crystal at the same temperature without an applied electric field, q_{11} and q_{12} are elements of the electrostriction tensor. For an isotropically strained film the in-plane misfit strain $u_m = u_{11} = u_{22}$:

$$u_m = u_{mR} + (\alpha_s - \alpha_f)(T - T_R) \tag{2.7.5}$$

Here α_s and α_f are the thermal expansion coefficients of the substrate and the film correspondingly, and u_{mR} is the misfit strain at a given temperature (typically at room T_R). The misfit strain at a given temperature may be measured using a grazing angle *X*-ray analysis:

$$u_{mR} = \frac{a_R - a_o}{a_o}, \tag{2.7.6}$$

where a_R is the measured in-plane lattice constant of the film, a_o is the lattice constant of the unstrained film, which is the same as the lattice constant of the bulk single crystal at temperature T_R. Alternatively, if the out-of-plane lattice constant c is available from the XRD analysis one may use the Poisson's ratio η to compute the in-plane strain:

$$u_{mR} = u_{33} \frac{1-\eta}{\eta}, \tag{2.7.7}$$

where u_{33} is the out-of plane strain:

$$u_{33} = \frac{c_R - c_o}{c_o} \tag{2.7.8}$$

The numerical values of the parameters for $SrTiO_3$ are given Table 2.7.1 (Tagantsev et al. 2005).

Table 2.7.1 Modal parameters for $SrTiO_3$

Ferroelectric parameters	η	q_{11}, m/F	q_{12}, m/F	Thermal expansion coefficient α, K^{-1}			
				$SrTiO_3$	MgO	Al_2O_3	Si
$SrTiO_3$	0.24	$2.2 \cdot 10^{10}$	$0.2 \cdot 10^{10}$	$11 \cdot 10^{-6}$	$13 \cdot 10^{-6}$	$6 \cdot 10^{-6}$	$4 \cdot 10^{-6}$

2.8 Electro-Acoustic Properties

2.8.1 Electrostriction

The term electrostriction is used describe electric field induced strain, i.e. fractional change of the sizes of a solid under applied electric field (2.7.2). In one dimensional case the strain is simply the ratio $u=\Delta a/a_o= \Delta l/l_o$, where l_o the original length of the sample, Δl is its change under the electric field. Electrostriction is general phenomena for all solids, however in ferroelectrics, especially near phase transition temperature, the effect is considerably larger. Electrostriction appears both in crystals with centrosymmetric lattice and in crystals without inversion symmetry, like ferroelectrics (e.g. $Ba_xSr_{1-x}TiO_3$) in paraelectric (cubic) and ferroelectric (tetragonal) phases. If the material is also piezoelectric the acoustic and electric properties are coupled via constitutive equations considered in the next section.

2.8.2 Piezoelectricity and Electrostriction

Ferroelectrics in polar (ferroelectric) phase, including complex oxides with perovskite structure, are piezoelectric. The indices used below correspond to axis notations shown in Fig. 2.7.3. The out-of plane (i.e. along axis 33) electric field displacement D_3 (C/m^2) and strain S_3 developed under the applied electric, E_3 (V/m), field, and stress, T_3 (N/m^2) are related via constitutive equations (Gonnard 2002):

$$D_3 = \varepsilon_{33}^T E_3 + d_{33} T_3 \tag{2.8.1}$$

$$S_3 = d_{33} E_3 + s_{33}^E T_3 \tag{2.8.2}$$

where P_3 is the polarization, the superscripts T and E stand for constant temperature and electric field (shorted electrodes), ε_{33} is the dielectric permittivity, s_{33} (m^2/N) is the elastic compliance, d_{33} (m/V=C/N) is the piezoelectric coefficient along 33 axes.

The electric field and strain developed under stress and displacement:

$$S_3 = s_{33}^D E_3 + g_{33} D_3 \tag{2.8.3}$$

$$E_3 = -g_{33} T_3 + \beta_{33}^T D_3 \tag{2.8.4}$$

with $g_{33} = d_{33}/\varepsilon_{33}$ (C/N=m/V). $\beta_{33} = 1/\varepsilon_{33}$ is the stiffness (inverse dielectric permittivity). The longitudinal coupling coefficient is defined as:

$$k_{33}^2 = d_{33}^2 / (s_{33}^T \varepsilon_{33}^E) = 1 - s_{33}^D / s_{33}^E \tag{2.8.5}$$

It shows the fraction of the electrical energy that covert into mechanical energy (and vice versa). In most of the practical cases the films deposited on a substrate are under interfacial (in-plane) strain T_1. In this case the associated relationships are:

$$S_1 = s_{11}^E T_1 + d_{31} E_3 \tag{2.8.6}$$

$$S_1 = s_{11}^D T_1 + g_{31} D_3 \tag{2.8.7}$$

$$D_3 = \varepsilon_{33}^T E_3 + d_{13} T_1 \tag{2.8.8}$$

$$E_3 = -g_{31} T_{13} + \beta_{33}^T D_3 \tag{2.8.9}$$

In the above relationships $g_{31}=d_{31}/s^T{}_{33}$,

$$k_{31}^2 = d_{31}^2 / (s_{33}^T \varepsilon_{11}^E) = 1 - s_{11}^D / s_{11}^E \tag{2.8.10}$$

The small signal losses are taken into account by assuming the dielectric permittivity, elastic compliance, and piezoelectric coefficient are complex quantities:

$$\varepsilon_{33} = \varepsilon_{33}^{'} - j\varepsilon_{33}^{''} = \varepsilon_{33}^{'}\left(1 - j \tan \delta_d\right) \tag{2.8.11}$$

$$s_{33} = s_{33}^{'} - j s_{33}^{''} = s_{33}^{'}\left(1 - j \tan \delta_m\right) \tag{2.8.12}$$

$$d_{33} = d_{33}^{'} - j d_{33}^{''} = d_{33}^{'}\left(1 - j \tan \delta_p\right) \tag{2.8.13}$$

where the real and imaginary parts of the parameters have standard meanings and the $tan\delta_d$, $tan\delta_m$, and $tan\delta_p$ are dielectric, mechanical (elastic) and piezoelectric loss tangents.

For a paraelectric film with no piezoelectric effect the piezoelectric coefficients $d_{33} = d_{31} = 0$. On the other hand it follows from (2.8.8) that in a polar, piezoelectric phase an in-plane strain T_1 will induce electric field via piezoelectric coefficient

d_{13} even with no applied electric field, $E_3 = 0$. One may expect a similar effect in films with paraelectric composition if a biaxial misfit strain induces piezoelectricity. Then a strain induced electric field may appear across the film normal to the substrate which may cause imprint in a parallel-plate capacitor even if the electrode/ferroelectric interfaces (potential barriers) are symmetric.

2.8.3 Electric Field Induced Piezoelectricity in Paraelectric Films

In general, one should not expect piezoelectric effect in crystals with center-symmetric crystal structure. However, the electromechanical study of single crystal *STO* (Rupprecht and Winner 1967) shows that the slight deviation from the ideal centrosymmetric-cubic structure, bulk single crystal STO exhibits a week piezoelectric effect with temperature, T, and electric field, E, dependences characterized by $\sim E/(T\text{-}Ta)$. Moreover, as it is indicated above the crystalline structure of the thin films having paraelectric composition (i.e. $Ba_xSr_{1-x}TiO_3$, $x<0.6$) is often far from being centrosymmetric due to the lattice mismatch and the mismatch in thermal expansion coefficients. A clamped by substrate and other interfacing layers film may experience additional lattice deformation due to electrostriction induced strains. Hence one may expect a substantial induced piezoelectric effect in thin films in comparison with the bulk single crystalline cubic counterparts. In (Tappe et al. 2004, Gevorgian et al. 2004) the piezoelectric effect in thin paraelectric films manifested itself as resonant absorption of microwave power, i.e. sharp increase in loss tangent at certain frequencies under increasing applied DC field. In summary, in paraelectric $Ba_xSr_{1-x}TiO_3$ films, the induced piezoelectric effect is associated with the strong electrostrictive effect. In paraelectric films there are no acoustic resonances without applied DC field. Under applied DC field the symmetry of the crystal is broken and for the superimposed RF signal the crystal pretends to be piezoelectric. In fact a thin film paraelectric capacitor with induced piezoelectricity acts as a Thin Film Bulk Acoustic Wave resonator (TFBAR). The simple theory of induced piezoelectricity in thin STO film given in (Gevorgian et al. 2006) explains the DC induced absorption peaks in parallel-plate $Ba_xSr_{1-x}TiO_3$ varactors. More advanced theories are proposed in (North et al. 2007, Vendik et al. 2008).

For an idealized TFBAR, assuming the thicknesses of the electrodes zero (no acoustic loading), the series resonance and parallel-resonance (anti-resonance) given in (Noeth et al. 2007) may be represented in simplified form:

$$f_p = \frac{1}{2t}\sqrt{\frac{c_{33}^D}{\rho}} \tag{2.8.14}$$

$$f_s = f_p\sqrt{1-8\frac{k_t^2}{\pi^2}} \tag{2.8.15}$$

where

$$k_t^2 = \frac{4q_{33}^2 \varepsilon_o \varepsilon_{33}^f(0) P_{DC}^{\ 2}}{c^D} \tag{2.8.16}$$

$$c^D = c^o - \left(m_{333} + 4q_{33}\varepsilon_o\varepsilon_b\right)P_{DC}^2 \tag{2.8.17}$$

P_{DC} is the polarization under applied DC field E_{DC}, i.e. $P_{DC}=\varepsilon_{33}(E)\varepsilon_o E_{DC}$, c^o, q_{33}, and m_{333} are corresponding components of the tensors of elastic constants ε_b is the background permittivity associated with the non-ferroelectric (non-soft mode) contribution in the dielectric permittivity, ρ is the density of the ferroelectric. The DC bias dependent real part of the permittivity, $\varepsilon_{33}(E)=\varepsilon(E, 300)$ may be calculated by (2.3.8) and any of appropriate formula given in Sects. 2.3 and 2.4. The numerical values of the acoustic parameters depend on the composition of the ferroelectric film quality, crystal orientation temperature etc. Currently they are being investigated and corrected. One has to keep in mind that the model described above is valid for small DC bias and RF fields. A similar model of induced piezoeffect is reported in (Vendik et al. 2008) where the second term in the brackets in (2.8.18) is missing.

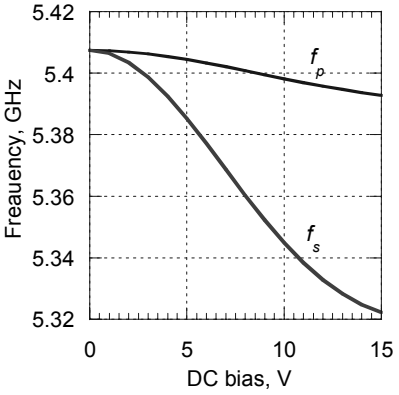

Fig. 2.8.1 Resonant frequencies for 0.5 μm thick $SrTiO_3$ assuming $C=8\cdot10^4\ K^{-1}$, $T=300$ K, $Tc=35.5$ K, $\beta=8\cdot10^9$ JC^{-4}m^{-5}, $m_{333}=-0.25\cdot10^{12}$, $c^o=3.16\cdot10^{11}$ N/m^2, $q_{33}=2.53\cdot10^{10}$ m/F, $\varepsilon_b=7$, $\rho=5130$ kg/m^3

The current temperature and composition dependent measurements on $Ba_xSr_{1-x}TiO_3$ (Berge et al. 2008) show that depending on temperature and composition the coefficient m_{333} may be positive or negative. The DC field dependent resonant frequencies calculated using (2.8.14), (2.8.15), (2.3.6) and (2.3.8) for a membrane based TFBAR are shown in Fig. 2.8.1. As it is expected from (2.8.15) the series resonant frequency is always smaller than the parallel one and its tuning is higher since it depends not only on the bias dependent c^D, but also on bias dependent k^2_t.

The impedance of the idealized (membrane based and infinite thin electrodes) TFBAR is:

$$Z = \frac{1}{j\omega C}\left[1 - k_t^2 \frac{\tan(\phi)}{\phi}\right] \tag{2.8.18}$$

Where $\phi = kt/2$, C is the DC dependent parallel-plate capacitance and t is the thickness of the ferroelectric film, and the k is the acoustic wave number:

$$k = \omega\sqrt{\frac{\rho}{c^D}} \tag{2.8.19}$$

2.9 Bulk Conductivity

In all ferroelectric devices the electrodes play a major role in their *I-V* performance. Additionally, the conductivity in ceramics is heavily affected by the grain boundaries. In this section only the basic conduction mechanisms in bulk single crystals are briefly outlined. The conductivity of the ferroelectric films and the leakage currents in ferroelectric varactors is discussed in Chap. 4, while the associated reliability and lifetime are addressed in Chap. 10.

Chemically (no impurities) and physically (no defects) clean ferroelectrics, i.e. $Ba_xSt_{1-x}TiO_3$, especially the quantum paraelectrics $SrTiO_3$, TiO_2, $KTaO_3$, $CaTiO3$, have rather high resistibility, typically more than 10^8 Ohm cm. To achieve high tuneabilities, in microwave devices based on ferroelectrics, the applied DC and often superimposed RF electric fields are very high. This is a typical situation in most thin film parallel-plate varactors. In the past the conductivity of the single crystal ferroelectrics studied mainly at relatively low electric fields. Recent experiments using very thin (77 nm) single crystal $BaTiO_2$ plates (Morrison et al. 2005) allowed to distinguish a number of conduction mechanisms characterized by different slops in I-V dependence.

Typically, below about 10 V/μm the conduction is negligible and the currents are dominated by injection of charge carriers over the electrode/ferroelectric barrier characterized by *exp(V/2KT)* dependence followed by a region with linear (not Ohmic) I-V dependence (Morrison et al. 2005).

Pool-Frenkel Effect: At relatively high temperature and electric field the conductivity may be associated with the Pool-Frenkel effect. The trapped electrons and holes are excited into shallow traps or conduction levels, due to the complex action of temperature and electric fields. In ferroelectric thin films the Pool-Frenkel emission becomes dominant above about 10V/μm, both in the surface layers and in the core of the ferroelectric film (Grossmann et al. 2002). Thus traps for electrons are assumed to be neutral when occupied and positive charged when empty (i.e., they are donors). Traps for holes are assumed to be neutral when emptied of an electron. Thus besides providing free charge carries the trapping/

detrapping results in changes in the charged states of the defects and hence contribute in the local polarization.

Hopping: This mechanism in $SrTiO_3$ (Fuchs et al. 2001) consider $I(E)=Aexp[(-(E/E^*)^{0.25}]$ current dependence where A is a temperature independent constant and E^* is a critical field. It is assumed that this conduction mechanism is active above 100–200 V/μm.

Space Charge Limited Currents (SCLC): It is shown in (Morrison et al. 2005) that in single crystal $BaTiO_3$ above 200 V/μm the currents are predominantly space charge limited.

2.10 Conclusions

Physics of the ferroelectrics, particularly for microwave applications, is rather well understood. The available models for the temperature, electric field and stress dependent permittivity, loss tangent and leakage currents are simple, rather correct and useful for development of scalable circuit models for ferroelectric varactors and complex microwave devices and systems based on them. At the same time the physical models are indispensable for the optimization of the synthesis process of the ferroelectric films, composites and fabrication devices.

References

Astafiev K F et al. (2005) Quasi-Debye microwave loss as an intrinsic limitation of microwave performance of tunable components based on $SrTiO_3$ and $Ba_xSr_{1-x}TiO_3$ ferroelectrics. J Appl Phys 97:014106-1- 014106-8

Barrett J H (1952) Dielectric Constant in Perovskite Type Crystals. Phys Rev 86:118

Berge J et al. (2008) Field and temperature dependent parameters of the dc field induced resonances in $Ba_xSr_{1-x}TiO_3$-based tunable thin film bulk acoustic resonators. J Appl Phys103:064508

Bete K (1970) Uber Das Mikrowellenverhalten Nichtlinearer Dielektrika. Philips Research Reports Supplements, vol 2

Chang W et al. (2005) In-plane anisotropy in the microwave dielectric properties of $SrTiO_3$ films. J Appl Phys 98:024107

Chosez P, Junquera J (2006) First-Principles Modeling of Ferroelectric Oxides Nanostructures. In: Rieth M, Schommers W (Ed) Handbook of Theoretical and Computational Nanotechnology. American Scientific Publisher, Stevenson Ranch California

Cochran W (1960) Crystal stability and theory of ferroelectricity. Adv Phys 9:387–423

Dawber M et al. (2005) Physics of thin film ferroelectric oxides. Rev Modern Phys 77:1083–1130

Eriksson A et al. (2003) Orientation and direct current field dependent dielectric properties of bulk single crystal $SrTiO_3$ at microwave frequencies. J Appl Phys 93:2848–2854

Fuchs D, Adam M, Schneider R (2001) Dielectric properties of Ti-deficient $SrTiO_{3-\delta}$ thin films. J. Physics IV France 11:71–76

Gevorgian S et al. (1997) HTS/Ferroelectric Devices for Microwave Applications. IEEE Appl Supercond 7(2):2458–2461

Gevorgian S et al. (2004) A Tuneable resonator. International Application No.: PCT/SE2004/001099, International Filing Date: 06.07.2004, Publication Date:12.01.2006 (WO 2006/004470 A1)

Gevorgian S et al. (2006) DC field and temperature dependent acoustic resonances in parallel-plate capacitors based on $SrTiO_3$ and $Ba_{0.25}Sr_{0.75}TiO_3$ films. Experiment and modeling. J Appl Phys 99:124112 (1–11)

Gonnard P (2002) Piezoelectric materials for high power applications: Electromechanical characterization and models. In: Setter N (Ed) Piezoelectric Materials and Devices, Ceramics Laboratory, EPFL, Lausanne

Grossmann M et al. (2002) The interface screening model as origin of imprint in $PbZr_xTi_{1-x}O_3$ thin films. Numerical simulation and verification. J Appl Phys 92(5):2688–2696

Haeni J H et al. (2004) Room temperature ferroelectricity in strained $SrTiO_3$. Nature 430:758–761

Hagenbeck R, Waser R (1999) Detailed temperature dependence of the space charge layer width at grain boundaries in acceptor doped $SrTiO_3$-ceramics. J Eur Ceramic Society, 19(6):683–686

Hemberger J et al. (1995) Electric field dependent dielectric constant and susceptibility in $SrTiO_3$. Phys Rev 52:1359–1362

Hemberger J et al. (1996) Quantum paraelectric and induced ferroelectric state in $SrTiO_3$. J Phys: Condens Matter 8:4673–4690

Hubert C et al. (1997) Confocal scanning optical microscopy of $Ba_xSr_{1-x}TiO_3$ thin films. Appl Phys Lett 71: 3353–3355

Lemanov V V et al. (1999) Perovskite $CaTiO_3$ as an incipient ferroelectric. Solid State Communications 110:611–614

McGibsson M M et al. (1996) The atomic structure of asymmetric tilt boundaries in $SrTiO_3$. Phyl Magazine A.73:625–641

Mishina E D et al. (2000) Observation of a Near-Surface Structural Phase Transition in $SrTiO_3$ by Optical Second Order Harmonic Generation. Phys Rev Lett 85 (17):3664–3667

Moon S E et al. (2003) Orientation dependent microwave dielectric properties of ferroelectric $Ba_{1-x}Sr_xTiO_3$ thin films. Appl Phys Lett 83:2166–2168

Morrison F D et al. (2005) High field conduction in barium titanate. Appl Phys Lett 86:152903

Muller K A, Burkard H (1979) $SrTiO_3$: An intrinsic quantum paraelectric below 4 K. Phys Rev B 19:3593–3602

Noeth A et al. (2007) DC bias—dependent shift of the resonant frequencies in BST film membranes. IEEE Utrasonics, Ferroelectrics and Frequency Control 54:2487–2492

North A et al. (2007) Tuning of direct current bias-induced resonances in $Ba_{0.3}Sr_{0.7}TiO_3$ micromachined thin film capacitors. J Appl Phys102:114110

Pertsev N A et al. (1998) Effect of mechanical boundary conditions on phase diagram of epitaxial ferroelectric thin films. Phys Rev Lett 80:1988–1991

Pertsev N A et al. (2000) Phase transitions and strain induced ferroelectricity in $SrTiO_3$ epitaxial films. Phys Rev B 61:R825–R829

Petzelt J et al. (2001) Polar grain boundaries in undoped $SrTiO_3$ ceramics. J Eur Cer Soci 21:2681–2686

Rupprecht G et al. (1961) Nonlinearity and Microwave Losses in Cubic Strontium-Titanate. Phys. Rev. 123 (1):97–98

Rupprecht G, Bell O (1962) Microwave Losses in Strontium Titanate Above Phase Transition. Phys Rev 125 (6):1915–1920

Rupprecht G, Bell O (1964) Dielectric Constant in Paraelectric Perovskites. Phys Rev135 (3A):A708–A752

Rupprecht G, Winner W H (1967) Electromechanical Behavior of Single-Crystal Strontium Titanate. Phys Rev155:1019–1028

Saad M (2004) Intrinsic dielectric response in ferroelectric nanocapacitors. J Phys Cond Matt 16:L451–L456

Stenge M, Spaldin N A (2006) Origin of the dielectric dead layer in nanoscale capacitors. Nature 443: 679–682

Su B, Button T (2004) Microstructure and Dielectric Properties of *Mg* doped barium strontium titanate ceramics. J Appl Phys 95 (3):1382–1385

Tagantsev A K (2005) Permittivity, tuneability and losses in ferroelectrics for reconfigurable high freauency electronics. In: Setter N (Ed) Electroceramic Based MEMs, Springer

Tagantsev A K and Glazunov A E (1998) Dielectric Nonlinearity and the nature of polarization response of PbMg1/3Nb2/3O3 reloaxor ferroelectric. J of the Korean Phys Soci 32:S951–S954

Tappe S et al. (2004) Electrostrictive resonances in $Ba_xSr_{1-x}TiO_3$ thin films at microwave frequencies. Appl Phys Lett 85:624–626

Vendik I B et al. (2008) Modeling tunable bulk acoustic wave resonators based on induced piezoelectric effect in and films. J Appl Phys103:014107

Vendik O G, Platonova L M (1971) Effect of charged lattice imperfections on the dielectric properties of materials. Sov Phys Solid State 13:1353–1359

Vendik O G, Ter-Martirosyan L T and Zubko S P (1998) Microwave losses in incipient ferroelectrics as functions of the temperature and the biasing field. J Appl Phys 84:993

Vendik O G, Zubko S P (1997) Modeling the dielectric response of incipient ferroelectrics. J Appl Phys 82:4475–4483

Vendik O G, Zubko S P (2000) Ferroelectric phase transition and maximum dielectric permittivity of displacement type ferroelectrics ($B_xSr_{1-x}TiO_3$). J Appl Phys 88:5343–5350

Vendik O G, Zubko S P, Nikol'ski M A (2002) Microwave loss-factor of $Ba_xSr_{1-x}TiO_3$ as a function of temperature, biasing field, barium concentration, and frequency. J Appl Phys 92:7448

Vendik O, Mironenko I, and Ter-Martirosyan L (1994) Superconductors Spur Applications of Ferroelectric Films. Microwaves & RF, July:67–70

http://www.springer.com/978-1-84882-506-2

Ferroelectrics in Microwave Devices, Circuits and Systems
Physics, Modeling, Fabrication and Measurements
Gevorgian, S.
2009, XX, 396 p., Hardcover
ISBN: 978-1-84882-506-2